Isothermal kinetics of carbothermic reduction of ilmenite concentrate with the addition of sodium carbonate

Xiaodong Lv [a, b], Dan Chen [a, b], Yuntao Xin [a, b*], Wei Lv [a, b], Jie Dang [a, b], Xuewei Lv [a, b*]

a. Chongqing Key Laboratory of Vanadium-Titanium Metallurgy and New Materials, Chongqing University, No. 174 Shazheng Street, Shapingba District, Chongqing 400044, PR China.
b. College of Materials Science and Engineering, Chongqing University, No. 174 Shazheng Street, Shapingba District, Chongqing, 400044 PR China.

** Corresponding Author:*
Professor Xuewei Lv, E-mail: lvxuewei@163.com
** Corresponding Author:*
Yuntao Xin, E-mail: xinyuntao0707@163.com

Abstract: In this study, the effect of the addition of Na_2CO_3 on the isothermal kinetics of carbothermic reduction of low-grade ilmenite concentrate is studied; this is a novel technique for obtaining high-quality upgraded titanium slag for chlorination through semi-molten states. The results indicate that the addition of Na_2CO_3 can reduce the initial temperature of the reaction and promote reduction, which is beneficial for improving the reaction kinetics by enhancing the carbon gasification reaction. The iron metal produced during the reaction tends to migrate and increase with the formation of the molten phase. The reduction of ilmenite concentrate gradually changes from being controlled by the interfacial chemical reaction to being controlled by diffusion with the increase in Na_2CO_3. At 0%, 3%, and 6% Na_2CO_3, the apparent activation energies were 105.01, 112.07, and 123.48 kJ/mol, respectively.

Keywords: Ilmenite concentrate; Isothermal kinetics; Sodium carbonate; Reduction

1. Introduction

Owing to its strong chemical activity, titanium naturally exists in the form of oxides, and it is often symbiotic with iron. In China, sources of titanium mainly include vanadium titanomagnetite, ilmenite concentrate, and other relatively low-grade titanium

sources. With the rapid development of the titanium industry, the reserves of high-grade titanium minerals are gradually being exhausted globally, and low-grade titanium sources are being used in industrial applications [1,2]. Electric furnace smelting is the major technology for producing titanium slag; however, the production efficiency is low and the energy consumption is high when low-grade ore is used in the process. [3-6]. Therefore, to produce high-quality titanium-rich materials for chlorination, a novel low-energy consumption process should be developed.

During the electric furnace smelting of titanium slag, effective separation of iron slag is the key step. In recent years, various studies have been conducted on the enhanced reduction of ilmenite concentrate by the use of additives. [7-15] Generally, it is believed that additives can enhance the reduction of ilmenite concentrate and facilitate the growth of metal particles. Studies on the kinetics of conventional carbothermal reduction [5,16-20], pre-oxidation reduction [21,22] and vacuum carbothermal reduction [23-25] of ilmenite concentrate have been conducted. In conventional reduction, the control models of the reaction are mainly interfacial chemical reaction control, diffusion control, and mixed control. In the carbothermal reduction of the original ilmenite concentrate and the pre-oxidized ilmenite concentrate, the average apparent activation energy of the pre-oxidized ilmenite concentrate is less than that of the original ilmenite concentrate by approximately 25%. [21]. The reduction of ilmenite concentrate in vacuum can reduce the initial temperature and increase the reaction rate. [26,27]

Therefore, based on previous studies, a low-energy process for producing high-quality upgraded titanium slag for chlorination is proposed by adding Na_2CO_3 to achieve a semi-melting condition for reduction. However, there are very few reports on the kinetics of the additive enhanced reduction of ilmenite concentrate, and the mechanism and kinetics of the reduction by the addition of Na_2CO_3 are further explored in this study.

2. Material and methods

2.1 Raw Materials

The chemical composition and the X-ray diffraction pattern of ilmenite concentrate used in the experiment are shown in **Table 2** and **Figure 1**, respectively, which indicates that the main phases in the ilmenite concentrate are $FeTiO_3$ and Fe_2O_3. The particle size analysis of ilmenite concentrate is shown in **Figure 2**. Most of the particles falls within

the range of 48–150 μm. The reducing agent used was graphite powder with ≥99.9 % purity and <13 μm particle size. The instrument used in the experiment was a high temperature silicon-molybdenum furnace with $MoSi_2$ as the heater, as shown in **Figure 3**.

Table1. Chemical composition of the ilmenite concentrate as pure oxides (wt%)

Compositions	TiO_2	FeO	Fe_2O_3	SiO_2	MnO	MgO	CaO	V_2O_5	Al_2O_3	P_2O_5	S
Content	45.73	32.41	17.09	2.68	0.78	0.59	0.26	0.198	0.163	0.094	<0.005

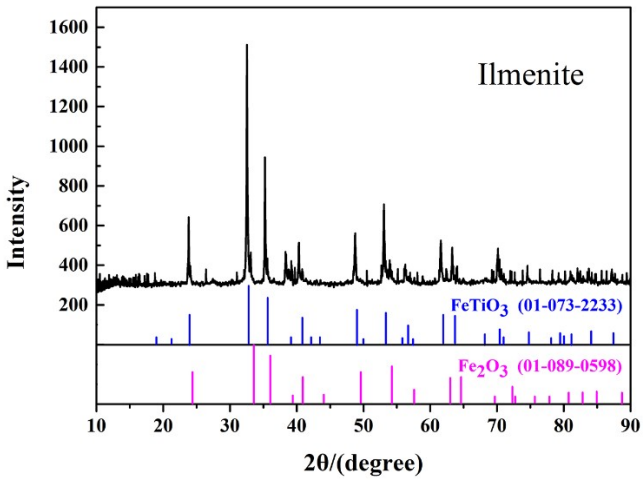

Fig. 1.XRD diagram of ilmenite concentrate

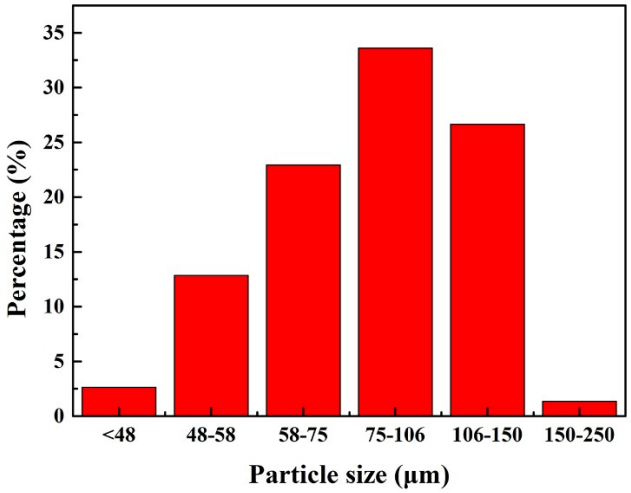

Fig.2 Analysis of size of ilmenite concentrate

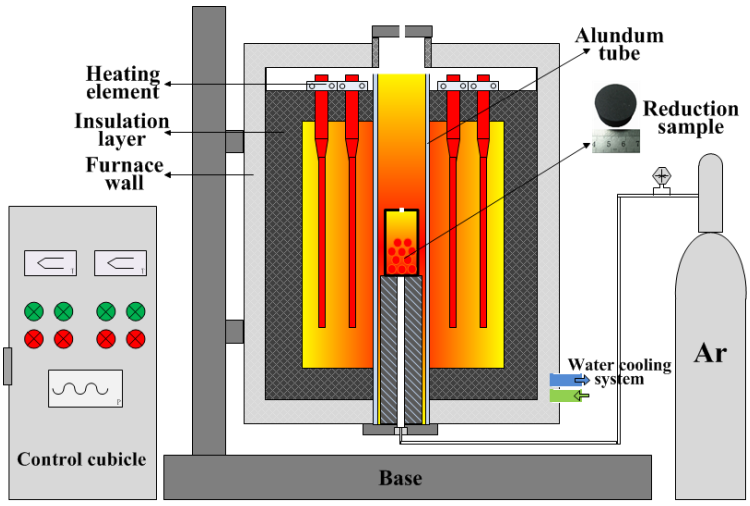

Fig. 3 Schematic diagram of high temperature silicon molybdenum furnace

2.2 Experimental procedure

The dosage of graphite powder was set as 13wt%, and that of the Na_2CO_3 additives was set at 0, 3 and 6wt%. The temperature was kept at 1373 K, 1423 K, 1473 K, 1523 K and 1573 K for 5min, 10min, 20min, 30min, 60min and 90min, respectively. All the materials were well mixed and then placed into a cylinder mold with a diameter of 16 mm to form tablets under the pressure of 8 Mpa, and the weight of the individual sample was 15 g. The sample was dried at 378 K for 120 min, and then the alumina crucible containing the sample tablet was placed in the furnace. The samples were quickly taken out for water cooling after the heating was finished, and then the samples were analyzed by XRD. In addition, the furnace was heated with a flowing argon gas (0.6 L/min, purity: 99.99 %).

Herein, in the isothermal reduction process, the reduction conversion degree is calculated as follows:

$$\alpha = \frac{\omega_o - \omega_t}{\omega_o - \omega_f}$$

Where α is the reduction degree, ω_o, $\omega_t$and ω_f represent the initial mass, the mass at time t, and the final mass of the sample with 100% reduction, respectively.

3. Results

3.1 Reduction degree analysis

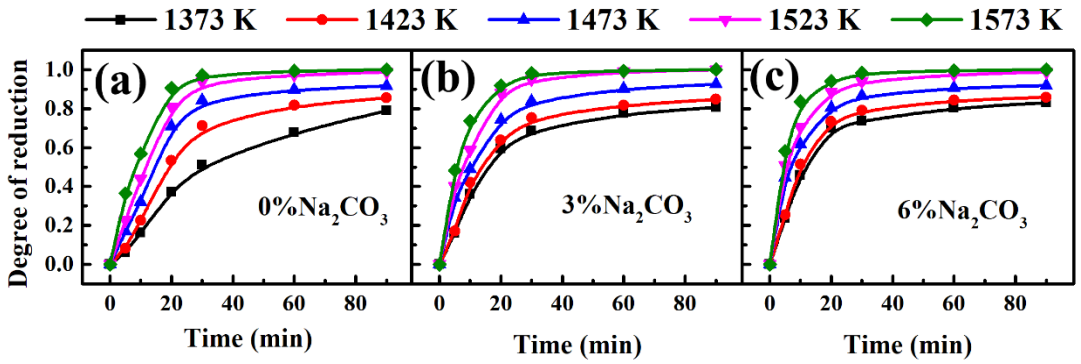

Fig. 4 Reduction degrees of reduced samples under different conditions ((a) 0% Na_2CO_3, (b) 3% Na_2CO_3, (c) 6% Na_2CO_3)

As shown in **Figure 4**, the reduction degree of the reduced sample increased with increasing amount of Na_2CO_3 at a constant temperature. This shows that the addition of Na_2CO_3 can promote reduction and enhance the reduction effect. For a similar amount of Na_2CO_3, the reduction degree of the sample increased with an increase in temperature; the increase in temperature improved the activity of reactants and promoted the reaction, causing the modified reduction to occur with an increase in temperature, which led to an increase in the reduction degree. At 1373 K, the addition of Na_2CO_3 significantly improved the reduction degree and promoted the reaction. At a temperature above 1423 K, reduction mainly occurred within the initial 30 min, and the degree of reaction changed slightly after that.

3.2 Phase transitions analysis

To explore the enhancement mechanism by the addition of Na_2CO_3 during the carbothermal reduction of ilmenite concentrate, X-ray diffraction (XRD) analysis was carried out on the reduced samples at different temperatures, time, and amount of Na_2CO_3, as shown in **Figure 5** and **Figure 6**.

When no Na_2CO_3 was added, diffraction peaks of TiO_2 were observed in the sample below 1473 K; when the temperature rose to 1473 K, the TiO_2 diffraction peaks disappeared and peaks of Ti_3O_5 appeared. When Na_2CO_3 was added, the diffraction peaks of TiO_2 disappeared, $Na_{0.23}TiO_2$ peaks appeared, and the strength of Ti_3O_5 peaks reduced. This indicates that the addition of Na_2CO_3 converted TiO_2 with a melting temperature of 2127 K to $Na_{0.23}TiO_2$ with a low melting temperature of 1238 K. [9,28], This prevented the

reduction to the high-melting temperature titanium suboxide (with a melting temperature of 2453 K),[2,17], thus enhancing the semi-molten effect and promoting the separation of metal from the slag.

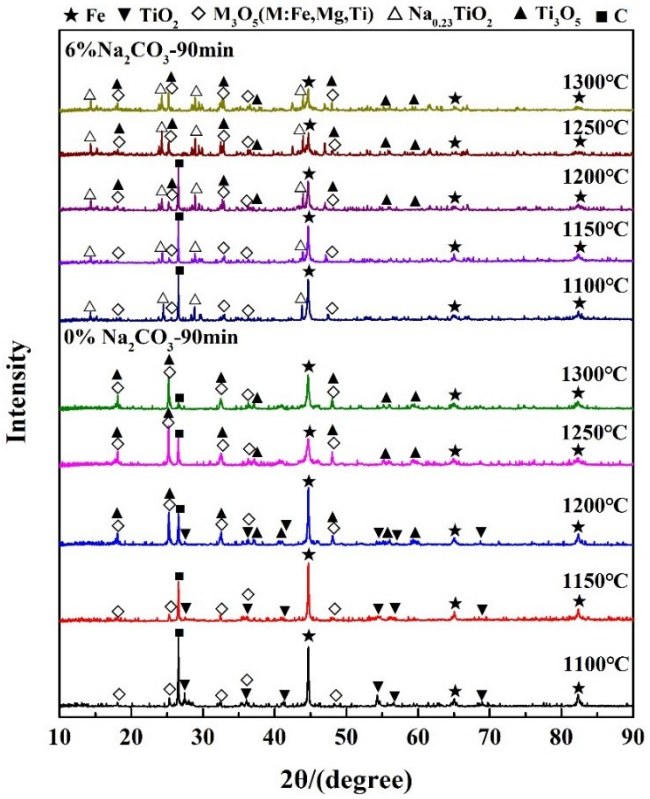

Fig. 5 Xrd patterns of reduced samples under different Na_2CO_3 samples with the change of temperature

Figure 6 shows that the $FeTiO_3$ peaks existed in the samples at a reduction temperature of 1473 K with a holding time of 10 min. However, the intensity of the peaks reduced after the addition of Na_2CO_3, indicating that Na_2CO_3 promoted the reduction reaction. When the holding time was 30 min, the $FeTiO_3$ peaks gradually disappeared and Ti_3O_5 peaks appeared; the peak of TiO_2 disappeared at the same time. The phase change of the reduced sample was not significant when the holding time exceeded 30 min; a solid solution (M_3O_5 (M: Fe, Mg, Ti, etc.)) was observed in the reduction sample, which was considered to affect the reduction effect.

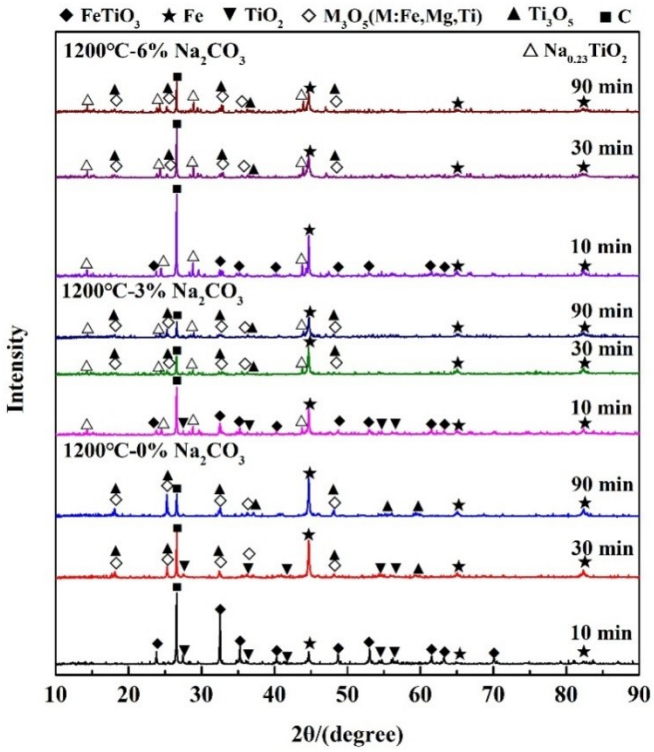

Fig. 6 Xrd patterns of reduced samples under different Na_2CO_3 samples with the change of time

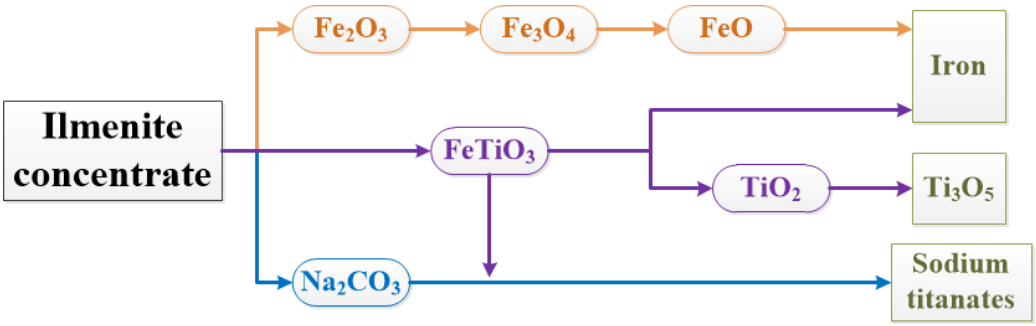

Fig. 7. Phase transitions of reduction of ilmenite concentrate enhanced by Na_2CO_3

As shown in **Figure 7**, the main phase transition in the reduction process can be analyzed from Fig. 4 and Fig. 5. The main phases of the ilmenite concentrate used in the experiment were Fe_2O_3 and $FeTiO_3$; therefore, the reduction process was as follows: $Fe_2O_3 \rightarrow Fe_3O_4 \rightarrow FeO \rightarrow Fe$ and $FeTiO_3 \rightarrow TiO_2 \rightarrow Ti_3O_5$. In addition, Na_2CO_3 decomposed into Na_2O and CO_2, and Na_2O reacted with TiO_2 to form sodium titanate with a low melting point. [9]

4. Discussion

4.1 Apparent activation energy analysis

According to **Figure 4** and the XRD analysis, the reduction mainly occurred within the first 30 min, after which the reaction degree changed only slightly; the complete reduction reaction and the migration and growth of the metallic iron essentially occurred within the initial 30 min. Therefore, only the processes that occurred during this duration were considered in the kinetics analysis. Generally, the "Mode fit method" is adopted to calculate the kinetics, wherein the experimental data is matched with the kinetics. [29-31]. The reduction degree under different conditions within 30 min (**Figure 4**) was substituted into different kinetic models for the calculation.[5,22,32,33] As shown in **Figure 8**, the best fitting degree was selected as the kinetics control condition. As indicated in **Figure 9** and Table 2, the apparent activation energy was obtained by the fit of the Arrhenius equation.[5,22] In addition, the relationship between the Gibbs free energy and temperature of the reaction equation was calculated using FactSage software, as shown in **Figure 10**.

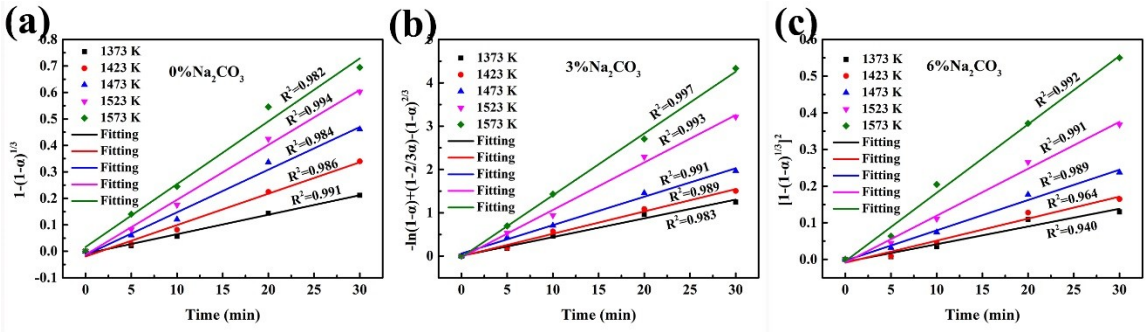

Fig. 8 Relationship between fitting diagrams of mechanism functions and reduction time under the different conditions ((a) 0% Na_2CO_3, (b) 3% Na_2CO_3, (c) 6% Na_2CO_3)

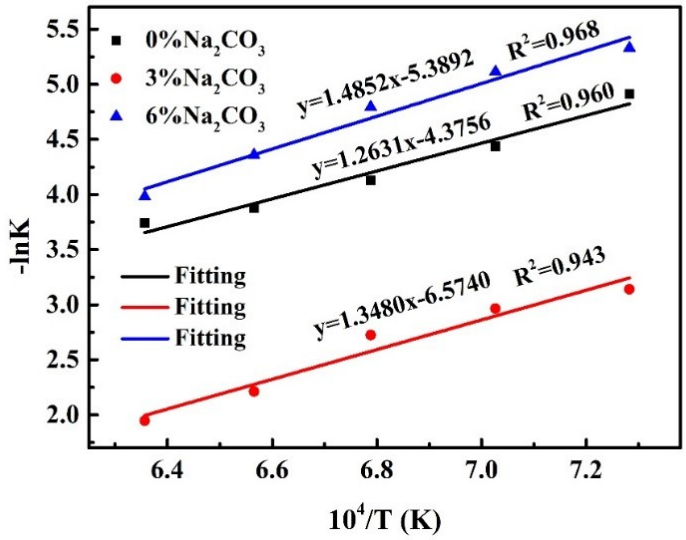

Fig. 9 Relationship between lnk and 1/T under different addition of Na_2CO_3

Table 2 Control model and kinetic parameter at different addition of Na_2CO_3

Na_2CO_3 additive	Control link	Kinetic models	G(α)	Ea (kJ/ mol)
0%	Interfacial chemical reaction control	Three-dimensional phase boundary reaction	$1-(1-\alpha)^{1/3}=kt$	105.01
3%	Mixed control of interfacial chemical reaction and diffusion	First-order reaction (Mample) Three-dimensional diffusion	$-ln(1-\alpha)=kt$ $(1-2/3\alpha)-(1-\alpha)^{2/3}=kt$	112.07
6%	Diffusion control	Three-dimensional diffusion	$[1-(1-\alpha)^{1/3}]^2=kt$	123.48

From Table 2, it is evident that as the amount of Na_2CO_3 increased, the reduction process of ilmenite gradually changed from being controlled by interfacial chemical reaction to being controlled by diffusion. When the Na_2CO_3 content was 0 %, the reduction reaction was controlled by the interfacial chemical reaction, which included the gasification reaction of carbon (Boudouard reaction [34]) and the reduction reaction of ilmenite. The corresponding kinetic model was represented by the integral expression function given by $G(a)=1-(1-\alpha)^{1/3}$, and the apparent activation energy was 105.01 kJ/mol.

When the Na_2CO_3 content was 3 %, it decomposed into Na_2O and CO_2 during heating; the Na_2O participated in the reaction of the ilmenite concentrate, thus reducing the Gibbs free energy of the reaction, as shown in **Figure 10**. Thus, the reaction occurred faster and at a lower temperature. The addition of Na_2CO_3 has a certain catalytic effect on

the carbon gasification reaction, which promotes the gasification of carbon,[35,36] thereby increasing the reaction rate and promoting the direct reduction of the ilmenite concentrate. Therefore, the interfacial chemical reaction was more efficient with the increase of Na_2CO_3 at a constant temperature, which reduced the possibility of interfacial reaction as a restrictive link during reduction. In addition, a molten phase was produced with the addition of Na_2CO_3, which reduced the diffusion rate of gas during reduction. Therefore, the reduction reaction was controlled by a combination of the interfacial chemical reaction and diffusion. The apparent activation energy slightly increased to 112.07 kJ/mol, and the kinetic model was represented by the integral expression function given by $G(a)=-ln(1-\alpha)+(1-2/3\alpha)-(1-\alpha)^{2/3}$. The molten phase increased as the Na_2CO_3 content increased to 6%, and the reduction reaction was controlled solely by diffusion control. The corresponding kinetics model was represented by the integral expression function given by $G(a)=[1-(1-\alpha)^{1/3}]^2$, and the apparent activation energy increased to 123.48 kJ/mol.

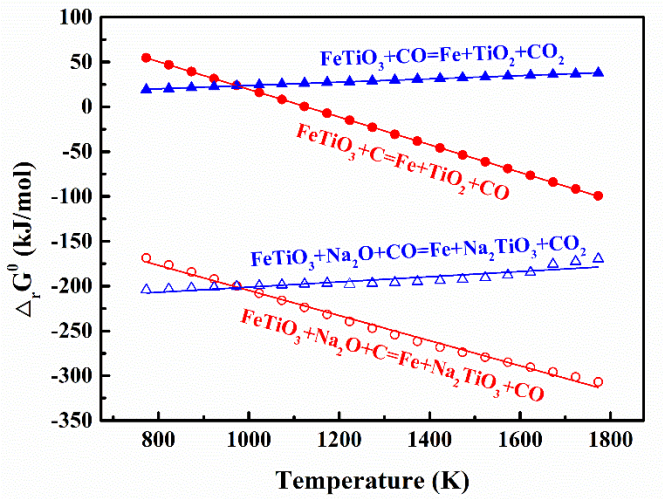

Fig. 10 Relationship between Gibbs free energy and temperature

4.2 Apparent activation energy contrastive analysis

Ilmenite is a complex solid solution, which can be expressed as follows: m[(Fe, Mg, Mn)O·TiO_2]·n[(Fe, Al, Cr)$_2O_3$], $m+n=1$, that is, the Fe^{2+} in ilmenite can be replaced by Mg^{2+} and Mn^{2+} of the isomorphism, and Fe^{3+} can be replaced by Al^{3+} and Cr^{3+} of the isomorphism. Therefore, there are several derivatives depending on the type and number of impurities in the ore, all of which have an effect on the reduction of minerals. The relationship between the Gibbs free energy and temperature of the major derivatives and

carbon is shown in **Figure 11**. The difficulty of reduction was in the following order: $CaO{\cdot}TiO_2$, $MgO{\cdot}TiO_2$, $MnO{\cdot}TiO_2$, and $FeO{\cdot}TiO_2$. Hence, the apparent activation energy of reduction of the various initial ilmenite concentrates was studied, and the corresponding values are summarized in Table 3. The chemical composition of the raw material is listed in Table 4.

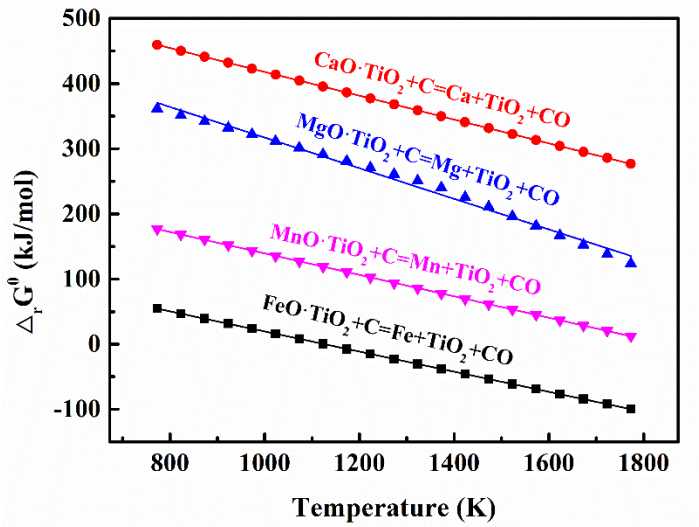

Fig. 11 Relationship of Gibbs free energy and temperature between the main derivatives and carbon

Table 3. Comparison of apparent activation energies from this research with those of previous researches

Raw materials	T (K)	Ea(kJ/mol)	Reference
Bama ilmenite concentrate, graphite	1123-1373	265	Wang et al.[19]
Ilmenite concentrate, charcoal	1273-1473	135	El-Tawil et al. [37]
Bama ilmenite concentrate, graphite	1373-1523	164	Wang et al.[19]
Ilmenite concentrate, graphite	1373-1573	105.01	This study
Bama ilmenite concentrate, graphite	1523-1673	157	Wang et al.[19]
Panzhihua ilmenite concentrate, graphite	1573-1773	219.2	Gou et al.[18]
Ilmenite concentrate with 3% Na_2CO_3, graphite	1373-1573	112.07	This study
Ilmenite concentrate with 6% Na_2CO_3, graphite	1373-1573	123.48	This study
Ilmenite concentrate with 30%	1273-1473	67	El-Tawil et al. [9]

	Na_2CO_3, charcoal

Table 4. Comparison of chemical composition of the raw material from this research with those of previous researches (wt%)

Reference	TiO_2	FeO	Fe_2O_3	SiO_2	MnO	MgO	CaO	Al_2O_3	Main phase
This study	45.73	32.41	17.09	2.68	0.78	0.59	0.26	0.16	$FeO·TiO_2$, Fe_2O_3
El-Tawil et al. [37]	42	24.79	28.81	2.98	0.16	-	-	-	$FeO·TiO_2$, Fe_2O_3
Wang et al. [19]	49.78	24.33	12.94	5.26	1.24	0.16	0.16	3.18	$FeO·TiO_2$, $Fe_2O_3·3TiO_2$
Gou et al. [18]	43.68	39.30	-	3.15	0.39	7.99	1.28	2.91	$FeO·TiO_2$

From Table 3 and Table 4, it can be observed that the raw materials investigated by El-Tawil et al.[37] and this study are mainly composed of ilmenite and hematite with low impurity content. In particular, the existence of hematite reduced the difficulty of mineral reduction and led to the low apparent activation energy. The raw materials studied by Wang et al. [19] are mainly composed of ilmenite and arizonite (formed after the weathering of ilmenite), which are difficult to reduce. In addition, the high content of Mn and Al in the raw materials increases the amount of solid solution and thus, the difficulty of reduction, as shown in **Figure 11**. Moreover, the existence of manganese oxide is detrimental to the reduction of iron oxide, [8] resulting in a high apparent activation energy. The highest apparent activation energy is presented by the raw material used by Gou et al., [18] which is composed of ilmenite with high contents of Ca and Mg. The greater the amount of impure oxides such as CaO and MgO in the raw material, the greater is the formation of compounds such as $CaO·TiO_2$ and $MgO·TiO_2$ with TiO_2; these compounds in turn form solid solutions with $FeO·TiO_2$, which increases the difficulty of reduction. Moreover, the existence of high Ca and Mg content inhibits the reduction kinetics of the ilmenite, making its reduction progressively difficult, with the inhibition effect even higher than that of manganese oxide. [8,38,39]. Furthermore, the reduction products can form a solid solution (M_3O_5 (M: Fe, Mg, Mn, Ti, etc.)), which hinders the reduction process. [38,40]. Generally, the apparent activation energy represents the difficulty of the reaction.

According to the above analysis, it can be concluded that the reduction difficulty of different raw materials was in the following order: the ilmenite with high Ca and Mg content > ilmenite > ilmenite with hematite.

As discussed above, a molten phase was produced with the addition of Na_2CO_3, which restricted the diffusion of CO, thus causing the reaction to have an increased apparent activation energy and become more difficult. However, compared with the study by El-Tawil et al., [9] the apparent activation energy of ilmenite was low when 30% Na_2CO_3 was added. This was because of the presence of a sufficient amount of Na_2O that participated in the reduction of ilmenite when excessive sodium carbonate was added, causing the rapid completion of the reaction and resulting in a low apparent activation energy.

4.3 Enhanced reduction mechanism analysis

The reduction mechanism of the ilmenite concentrate enhanced by Na_2CO_3 is shown in **Figure 12**. In the conventional reduction process, solid minerals surrounded the reaction nucleus in the early stage of the reaction. Therefore, the reduction reaction mainly occurred through direct contact with the reductants. As the reaction progressed, the product layer generated via reduction surrounded the reaction nucleus, and the reductant needed to migrate to the surface of the reaction nucleus through the diffusion channel to continue the reaction. The iron produced during the reaction formed a dense metal shell surrounding the reaction core, which hindered the migration of the reducing agent, thus affecting the reduction process.

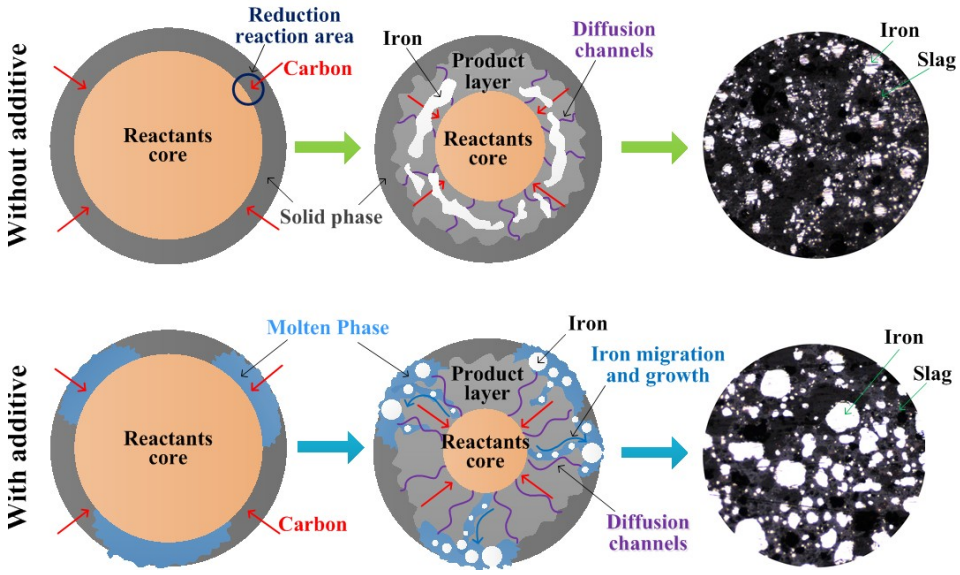

Fig. 12 Mechanism diagram of ilmenite concentrate reduction enhanced by Na_2CO_3

When Na_2CO_3 was added, the Na_2O produced via the decomposition of Na_2CO_3 reacted with TiO_2 to form sodium titanates with a low melting point, and the reaction nucleus was surrounded by the molten phase. Although an increased amount of the molten phase restricted the diffusion of CO and hindered the reaction, the reaction progressed efficiently at the beginning and at a low temperature, where the molten phase was beneficial to the diffusion and migration of particles; the reductant rapidly diffused to the surface of the reaction nucleus through the migration channel in the molten phase to participate in the reduction reaction, thus increasing the reaction rate. In addition, the iron produced during reduction migrated to the molten phase, and accumulated to form metal particles. Thus, no dense iron shell was formed surrounding the reactants, and the contact probability between the reaction nucleus and reducing agent increased in the presence of the molten phase; this in turn increased the probability of reaction and promoted the reduction reaction. The addition of Na_2CO_3 not only promoted the reaction, but also the nucleation growth of the metallic iron, thus facilitating the subsequent separation of metal from the slag.

5. Conclusion

(1) Both, the increase in the temperature and the extension of the holding time, are important for improving the reduction reaction. The addition of Na_2CO_3 can reduce the initial temperature of the reaction and produce a molten phase, which is beneficial for the reaction kinetics between the reaction core and the reducing agent, and enhances the

reduction effect. The iron metal produced during the reaction tends to migrate and grow with the formation of the molten phase.

(2) The formation of the molten phase was detrimental to the diffusion of gas, and the reduction process gradually changed from being controlled by interfacial chemical reaction to being controlled by diffusion as the amount of Na_2CO_3 increased. When the amounts of Na_2CO_3 were 0%, 3%, and 6%, the reduction reaction was controlled by interfacial chemical reaction, a combination of interfacial chemical reaction and diffusion, and diffusion, respectively. The corresponding kinetic models were expressed by the following functions: $G(a)=1-(1-\alpha)^{1/3}$, $G(a)=-ln(1-\alpha)+(1-2/3\alpha)-(1-\alpha)^{2/3}$, and $G(a)=[1-(1-\alpha)^{1/3}]^2$, and the apparent activation energies were 105.01, 112.07, and 123.48 kJ/mol, respectively.

(3) The type and amount of impurities in the raw material affect the reduction of minerals; hematite as a constituent material and low contents of impurities such as Ca and Mg reduce the difficulty of reduction, which leads to low apparent activation energy and easy reduction of minerals. The difficulty of reduction based on the content of raw material was in the following order: the ilmenite with high Ca and Mg content > ilmenite > ilmenite with hematite.

Acknowledgments

This work was supported by the National Natural Science Foundation of China (Grant No. U1902217).

REFERECES

1. Kucukkaragoz CS, Eric RH. Solid state reduction of a natural ilmenite. *Miner Eng.* 2006;19(3):334-337.
2. Huang R, Lv XW, Bai CG, Deng QY, Ma SW. Solid state and smelting reduction of Panzhihua ilmenite concentrate with coke. *Can Metall Q.* 2012;51(4):434-439.
3. Dang J, Zhang G, Chou K. Kinetics and mechanism of hydrogen reduction of ilmenite powders. *JAllC.* 2015;619:443-451.
4. Gou H, Zhang G, Chou K. Influence of pre-oxidation on carbothermic reduction process of ilmenite concentrate. *ISIJ Int.* 2015;55(5):928-933.
5. Zhang Y, Lv W, Lv X, et al. Isothermal reduction kinetics of Panzhihua ilmenite concentrate under 30vol% CO-70vol% N-2 atmosphere. *International Journal of Minerals Metallurgy and Materials.* 2017;24(3):240-248.
6. Wu F, Li X, Wang Z, et al. Hydrogen peroxide leaching of hydrolyzed titania residue prepared

from mechanically activated Panzhihua ilmenite leached by hydrochloric acid. *Int J Miner Process.* 2011;98(1-2):106-112.
7. Gupta SK, Rajakumar V, Grieveson P. Kinetics of reduction of ilmenite with graphite at 1000 to 1100 °C. *Metall Mater Trans B.* 1987;18(4):713-718.
8. Gupta SK, Rajakumar V, Grieveson P. The influence of weathering on the reduction of llmenite with carbon. *Metall Trans B.* 1989;20B:735-745.
9. ElTawil SZ, Morsi IM, Yehia A, Francis AA. Alkali reductive roasting of ilmenite ore. *Can Metall Q.* 1996;35(1):31-37.
10. Li G, Shi T, Rao M, Jiang T, Zhang Y. Beneficiation of nickeliferous laterite by reduction roasting in the presence of sodium sulfate. *Miner Eng.* 2012;32:19-26.
11. Huang R, Lv X, Bai C, Zhang K, Qiu G. Enhancement reduction of panzhihua ilmenite concentrate with coke and conglomeration of metal with ferrosilicon. *Steel Res Int.* 2013;84(9):892-899.
12. Geng C, Sun T, Yang H, Ma Y, Gao E, Xu C. Effect of Na_2SO_4 on the embedding direct reduction of beach titanomagnetite and the separation of titanium and iron by magnetic separation. *ISIJ Int.* 2015;55(12):2543-2549.
13. Song B, Lv X, Miao HH, Han K, Zhang K, Huang R. Effect of $Na_2B_4O_7$ addition on carbothermic reduction of ilmenite concentrate. *ISIJ Int.* 2016;56(12):2140-2146.
14. Lv W, Bai C, Lv X. Carbothermic reduction of ilmenite concentrate in semi-molten state by adding sodium sulfate. *Powder Technol.* 2018;340:354-361.
15. Kimura S, Smith JM. Kinetics of the sodium carbonate-sulfur dioxide reaction. *AICHE J.* 1987;33(9):1522-1532.
16. Saensunon B, Stewart GA, Pax R. A combined Fe-57-Mossbauer and X-ray diffraction study of the ilmenite reduction process in a commercial rotary kiln. *Int J Miner Process.* 2008;86(1-4):26-32.
17. Pourabdoli M, Raygan S, Abdizadeh H, Hanaei K. Production of high titania slag by Electro-Slag Crucible Melting (ESCM) process. *Int J Miner Process.* 2006;78(3):175-181.
18. Gou H, Zhang G, Chou K. Phase evolution during the carbothermic reduction process of ilmenite concentrate. *Metall Mater Trans B.* 2015;46(1):48-56.
19. Wang YM, Yuan ZF, Guo ZC, Tan QQ, Li ZY, Jiang WZ. Reduction mechanism of natural ilmenite with graphite. *Transactions of Nonferrous Metals Society of China.* 2008;18(4):962-968.
20. Zhao Y, Shadman F. Kinetics and mechanism of ilmenite reduction with carbon monoxide. *AICHE J.* 1990;36(9):1433-1438.
21. Lv W, Lv X, Xiang J. Effect of pre-oxidation on the carbothermic reduction of ilmenite concentrate powder. *Int J Miner Process.* 2017;169:176-184.
22. Lv W, Lv X, Zhang Y, Li S, Tang K, Song B. Isothermal oxidation kinetics of ilmenite concentrate powder from Panzhihua in air. *Powder Technol.* 2017;320:239-248.
23. Huang R, Lv X, Wu Q, Wu Q, Zhang J. Non-isothermal reduction kinetics of iron during vacuum carbothermal reduction of ilmenite concentrate. *Metall Mater Trans B.* 2019;50(2):816-824.
24. Lv X, Huang R, Wu Q, Xu B, Zhang J. Non-isothermal reduction kinetics during vacuum carbothermal reduction of ilmenite concentrate. *Vacuu.* 2019;160:139-145.
25. Lv X, Huang R, Wu Q, Wu Q, Zhang J. Volatilisation behaviour of iron, silicon and magnesium during vacuum carbothermal reduction of ilmenite concentrate. *Can Metall Q.* 2019;58(4):419-426.
26. Huang R, Liu P, Qian X, Zhang J. Comprehensive utilization of Panzhihua ilmenite concentrate by vacuum carbothermic reduction. *Vacuu.* 2016;134:20-24.
27. Huang R, Liu P, Zhang J, Yue Y. Effects of temperature on vacuum carbothermic reduction of Panzhihua ilmenite concentrate. *Metallurgist.* 2017;61(5-6):511-516.
28. Lv W, Lv X, Xiang JY, Zhang Y, Li SP. A novel process to prepare high-titanium slag by carbothermic reduction of pre-oxidized ilmenite concentrate with the addition of Na_2SO_4. *Int J Miner Process.* 2017;167:68-78.
29. Starink MJ. The determination of activation energy from linear heating rate experiments: a comparison of the accuracy of isoconversion methods. *Thermochim Acta.* 2003;404(1-2):163-176.
30. Starink MJ. Activation energy determination for linear heating experiments: deviations due to neglecting the low temperature end of the temperature integral. *JMatS.* 2007;42(2):483-489.
31. Kharatyan SL, Chatilyan HA, Mukasyan AS, Simonetti DA, Varma A. Effect of heating rate on

kinetics of high-temperature reactions: Mo-Si system. *AICHE J.* 2005;51(1):261-270.
32. Li P, Yu Q, Qin Q, Lei W. Kinetics of CO_2/coal gasification in molten blast furnace slag. *Ind Eng Chem Res.* 2012;51(49):15872-15883.
33. Li P, Yu Q, Xie H, Qin Q, Wang K. CO_2 gasification rate analysis of datong coal using slag granules as heat carrier for heat recovery from blast furnace slag by using a chemical reaction. *Energy Fuels.* 2013;27(8):4810-4817.
34. Elguindy MI, Davenport WG. Kinetics and mechanism of ilmenite reduction with graphite. *Metall Mater Trans B.* 1970;1(6):1729-1734.
35. Mckee DM. Mechanisms of the alkali metal catalysed gasification of carbon. *Fuel.* 1983;62:170-175.
36. Wood BJ, Fleming RH, Wise H. Reactive intermediate in the alkali-carbonate-catalysed gasification of coal char. *Fuel.* 1984;63(11):1600-1603.
37. Eltawil SZ, Morsi IM, Francis AA. Kinetics of solid-state reduction of ilmenite ore. *Can Metall Q.* 1993;32(4):281-288.
38. Wang Y, Yuan Z. Reductive kinetics of the reaction between a natural ilmenite and carbon. *Int J Miner Process.* 2006;81(3):133-140.
39. Merk R, Pickles CA. Reduction of ilmenite by carbon-monoxide. *Can Metall Q.* 1988;27(3):179-185.
40. Bessinger D, Geldenhuis JMA, Pistorius PC, Mulaba A, Hearne G. The decrepitation of solidified high titania slags. *J Non-Cryst Solids.* 2001;282(1):132-142.

Figure Captions:

Fig. 1.XRD diagram of ilmenite concentrate

Fig.2 Analysis of size of ilmenite concentrate

Fig. 3 Schematic diagram of high temperature silicon molybdenum furnace

Fig. 4 Reduction degrees of reduced samples under different conditions ((a) 0% Na_2CO_3, (b) 3% Na_2CO_3, (c) 6% Na_2CO_3)

Fig. 5 Xrd patterns of reduced samples under different Na_2CO_3 samples with the change of temperature

Fig. 6 Xrd patterns of reduced samples under different Na_2CO_3 samples with the change of time

Fig. 7. Phase transitions of reduction of ilmenite concentrate enhanced by Na_2CO_3

Fig. 8 Relationship between fitting diagrams of mechanism functions and reduction time under the different conditions ((a) 0% Na_2CO_3, (b) 3% Na_2CO_3, (c) 6% Na_2CO_3)

Fig. 9 Relationship between lnk and 1/T under different addition of Na_2CO_3

Fig. 10 Relationship between Gibbs free energy and temperature

Fig. 11 Relationship of Gibbs free energy and temperature between the main derivatives and carbon

Fig. 12 Mechanism diagram of ilmenite concentrate reduction enhanced by Na_2CO_3

Table Captions:

Table 1. Chemical composition of the ilmenite concentrate as pure oxides (wt%)

Table 2. Control model and kinetic parameter at different addition of Na_2CO_3

Table 3. Comparison of apparent activation energies from this research with those of previous researches

Table 4. Comparison of chemical composition of the raw material from this research with those of previous researches (wt%)